

Article

A Novel Comprehensive Scheme for Vehicle State Estimation Using Dual Extended H-Infinity Kalman Filter

Fengjiao Zhang ^{1,2,*}, Yan Wang ², Jingyu Hu ², Guodong Yin ², Song Chen ¹, Hongdang Zhang ¹ and Dong Zhou ³

¹ School of Vehicle Engineering, Changzhou Vocational Institute of Mechatronic Technology, Changzhou 213164, China; cs2208@czimt.edu.cn (S.C.); zhd1901@czimt.edu.cn (H.Z.)

² School of Mechanical Engineering, Southeast University, Nanjing 211189, China; yanwangiv@seu.edu.cn (Y.W.); 220190313@seu.edu.cn (J.H.); ygd@seu.edu.cn (G.Y.)

³ School of Field Engineering, Army Engineering University of PLA, Nanjing 210007, China; zd2020066@163.com

* Correspondence: zfj2185@czimt.edu.cn

Abstract: The performance of vehicle active safety systems relies on accurate vehicle state information. Estimation of vehicle state based on onboard sensors has been popular in research due to technical and cost constraints. Although many experts and scholars have made a lot of research efforts for vehicle state estimation, studies that simultaneously consider the effects of noise uncertainty and model parameter perturbation have rarely been reported. In this paper, a comprehensive scheme using dual Extended H-infinity Kalman Filter (EH ∞ KF) is proposed to estimate vehicle speed, yaw rate, and sideslip angle. A three-degree-of-freedom vehicle dynamics model is first established. Based on the model, the first EH ∞ KF estimator is used to identify the mass of the vehicle. Simultaneously, the second EH ∞ KF estimator uses the result of the first estimator to predict the vehicle speed, yaw rate, and sideslip angle. Finally, simulation tests are carried out to demonstrate the effectiveness of the proposed method. The test results indicate that the proposed method has higher estimation accuracy than the extended Kalman filter.

Keywords: vehicle state estimation; extended H-infinity Kalman filter; noise uncertainty; model parameter perturbation



check for updates

Citation: Zhang, F.; Wang, Y.; Hu, J.; Yin, G.; Chen, S.; Zhang, H.; Zhou, D. A Novel Comprehensive Scheme for Vehicle State Estimation Using Dual Extended H-Infinity Kalman Filter. *Electronics* **2021**, *10*, 1526. <https://doi.org/10.3390/electronics10131526>

Academic Editor: Giambattista Grusso

Received: 1 June 2021
Accepted: 15 June 2021
Published: 24 June 2021

Publisher's Note: MDPI stays neutral with regard to jurisdictional claims in published maps and institutional affiliations.



Copyright: © 2021 by the authors. Licensee MDPI, Basel, Switzerland. This article is an open access article distributed under the terms and conditions of the Creative Commons Attribution (CC BY) license (<https://creativecommons.org/licenses/by/4.0/>).

1. Introduction

1.1. Motivation

Active safety systems have proven themselves to be one of the most effective means of reducing traffic accidents. Some typical active safety systems include antilock braking systems [1], yaw stability systems [2], collision avoidance systems [3], and so on. The prerequisite for these active safety systems to work accurately is the availability of accurate vehicle state information [4]. Existing onboard sensors are limited in the number of vehicle states they can measure. Some states that characterize vehicle stability, such as the sideslip angle, cannot be measured by onboard sensors. Although some special sensors can measure the sideslip angle, they are expensive and require additional installation in mass production cars, which greatly limits the application of this measurement method. To obtain some key state information of the vehicle more economically, many scholars have proposed various interesting estimation methods.

1.2. Literature Review and Limitations

In recent years, the studies of estimation methods based on nonlinear observer and Kalman filter (KF) have been widely reported. In the literature [5–8], the method based on a nonlinear observer is used to estimate the vehicle state and is proved to be effective under certain conditions. However, the estimation accuracy of the nonlinear observer is heavily

dependent on the accuracy of the vehicle model parameters. In addition, Kalman filter-based estimation methods are widely used in vehicle positioning, navigation, and control due to their ability to efficiently handle measurement noise [9]. Its iterative process consists of three steps. Firstly, the statistical properties of the system noise and the observation noise are used to process the time update and the observation update of the random signal, then the unknown variables are estimated, and finally, the optimal estimate is achieved [10].

In general, the traditional KF is only suitable for linear systems. It requires that the observation equation is linear [11]. Thus, it is not suitable for the state estimation of complicated and nonlinear vehicle systems. On the other hand, the traditional KF requires that the model parameters and noise variances are precisely known [12]. Furthermore, the process noise and measurement noise are white noises and are uncorrelated with each other [13]. In many practical applications, system model parameters and/or noise variance often are uncertainties because of model perturbation, stochastic disturbance, and unmodeled dynamics [14]. These factors usually deteriorate the estimation accuracy of KF.

Therefore, extended Kalman filtering [15–17] is proposed to deal with these problems. Some studies have shown that EKF has better estimation accuracy compared to KF [18–22]. However, when statistical properties of noise are unknown, the estimation accuracy of EKF will decrease. Thus, some scholars proposed the adaptive extended Kalman filter (AEKF) [23,24]. When the system noise is unknown, the AEKF-based solution can obtain more accurate vehicle states. In addition, some researchers attempt to utilize the H-infinity filter to estimate the vehicle states with noise uncertainties. In [25], the H-infinity filter was used to weaken the effect of noise uncertainty on the estimation accuracy. In addition, state estimation considering parameter perturbation is an interesting research hotspot. The model parameters to be identified will vary according to the complexity of the vehicle dynamics model. For example, considering vehicle drive conditions, some driveline parameters need to be obtained. Montonen et al. [26,27] identified the mechanical driveline parameters of a hybrid bus by inputting a pseudo-random binary signal. Furthermore, some scholars have proposed a comprehensive estimation architecture [6,28,29]. It generally consists of two parts: one is the online estimation of the parameters of the model, and the other is the use of various filtering algorithms to obtain better estimation performance based on the updated model.

Although a lot of research work has been done by many experts and scholars for the above problems, few studies have been reported considering both noise uncertainty and model parameter perturbation. Thus, in the paper, we propose a novel comprehensive scheme for vehicle state estimation. The main contributions of this article are as follows. A comprehensive scheme using dual EKF is proposed to estimate the vehicle mass and vehicle state when the noise statistics are unknown and model parameters are inaccurate. Furthermore, the virtual tests show that the proposed method can acquire higher estimation accuracy than the existing EKF. The remainder of this paper is structured as follows. The vehicle model is introduced in Section 2. Section 3 presents the proposed comprehensive scheme in detail. Section 4 shows the virtual test results. Finally, Section 5 concludes this work.

2. Vehicles Dynamics Estimation Models

Considering real-time computing requirements and estimator design issues, a nonlinear three-degree of freedom vehicle model (see Figure 1) is used for the vehicle state and parameter estimation [30]. In order to handle a tractable estimation problem using only the standard sensors, we have to make some assumptions. The steering angles of the front left and right wheels are the same. The left and right wheels on each axle have the same stiffness. The lateral forces are decoupled from the longitudinal forces. The effects of wind and air resistance are neglected. Its equations of motion are as follows:

$$\begin{cases} \dot{\gamma} = \frac{a^2k_1+b^2k_2}{I_z v_x} \gamma + \frac{ak_1-bk_2}{I_z} \beta - \frac{ak_1}{I_z} \delta \\ \dot{\beta} = \left(\frac{ak_1-bk_2}{m v_x^2} - 1\right) \gamma + \frac{k_1+k_2}{m v_x} \beta - \frac{k_1}{m v_x} \delta \\ \dot{v}_x = \gamma \beta v_x + a_x \end{cases} \quad (1)$$

$$a_y = \frac{ak_1 - bk_2}{m v_x} \gamma + \frac{k_1 + k_2}{m} \beta - \frac{k_1}{m} \delta \quad (2)$$

where γ , β are respectively yaw rate and sideslip angle; v_x and v_y are respectively longitudinal vehicle speed and lateral vehicle speed; a and b are respectively distance from the center of gravity to the front axle and distance from the center of gravity to the rear axle; L is the wheelbase; F_{x1} and F_{y1} are respectively longitudinal and lateral forces on the front axle; F_{x2} and F_{y2} are respectively longitudinal and lateral forces on the rear axle; k_1 and k_2 are respectively cornering stiffness of the front axle and cornering stiffness of the rear axle; I_z and m are respectively vehicle moment of inertia about z axis and vehicle mass; a_x and a_y are respectively longitudinal acceleration and lateral acceleration; and δ is front-wheel steering angle.

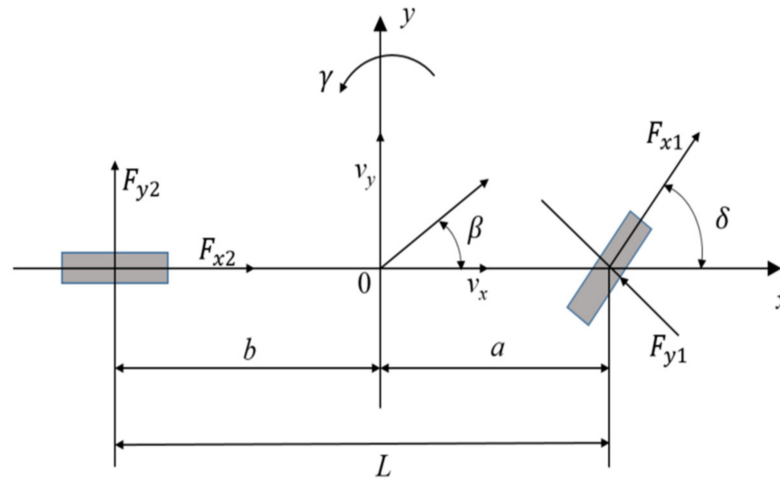


Figure 1. The nonlinear three degrees of freedom vehicle model.

State and measurement equations of the vehicle model, that is, Formulations (1) and (2) can be converted to a continuous-time state-space model.

$$\begin{cases} \dot{x}(k) = f(x(k), u(k), w(k)) \\ y(k) = h(x(k), u(k), v(k)) \end{cases} \quad (3)$$

where $x(k)$, $u(k)$, and $y(k)$ are respectively state vector, input vector, and measurement vector, for mass estimation: $x(k) = [m]^T$ and $y(k) = [a_y]^T$; for state estimation: $x(k) = [\gamma, \beta, v_x]^T$, $u(k) = [\delta, a_x]^T$, and $y(k) = [a_y]^T$; $w(k)$ and $v(k)$ are respectively the state process noise and measurement noise; $f(\cdot)$ and $h(\cdot)$ are respectively the state transition and output function.

It is necessary to discretize the continuous-time vehicle model to accomplish the estimation of vehicle states via discrete measurements. Equation (3) can be written as follows:

$$\begin{cases} x(k+1) = f(x(k), u(k)) + w(k) \\ y(k+1) = h(x(k+1), u(k+1)) + v(k+1) \end{cases} \quad (4)$$

For mass estimation, $x(k+1) = [m_{k+1}]^T$, $y(k+1) = [a_{y,k+1}]^T$, $\Delta(k)$ is the sample time. The nonlinear vehicle system can be written as follows:

$$[m_{k+1}]^T = [m_k]^T \quad (5)$$

$$[a_{y,k}]^T = \left[\frac{ak_1 - bk_2}{mv_{x,k}} \gamma_k + \frac{k_1 + k_2}{m} \beta_k - \frac{k_1}{m} \delta_k \right]^T \tag{6}$$

For state estimation, $x(k + 1) = [\gamma_{k+1}, \beta_{k+1}, v_{x,k+1}]^T$, $y(k + 1) = [a_{y,k+1}]^T$. The nonlinear vehicle system can be written as follows:

$$\begin{bmatrix} \gamma_{k+1} \\ \beta_{k+1} \\ v_{x,k+1} \end{bmatrix} = \begin{bmatrix} \gamma_k + \left(\frac{a^2k_1 + b^2k_2}{I_z v_{x,k}} \gamma_k + \frac{ak_1 - bk_2}{I_z} \beta_k - \frac{ak_1}{I_z} \delta_k \right) \Delta k \\ \beta_k + \left[\left(\frac{ak_1 - bk_2}{mv_{x,k}^2} - 1 \right) \gamma_k + \frac{k_1 + k_2}{mv_{x,k}} \beta_k - \frac{k_1}{mv_{x,k}} \delta_k \right] \Delta k \\ v_{x,k} + (\gamma_k \beta_k v_{x,k} + a_{x,k}) \Delta k \end{bmatrix} \tag{7}$$

$$[a_{y,k}]^T = \left[\frac{ak_1 - bk_2}{mv_{x,k}} \gamma_k + \frac{k_1 + k_2}{m} \beta_k - \frac{k_1}{m} \delta_k \right]^T \tag{8}$$

3. Methodology

The framework of the proposed comprehensive scheme is presented in Figure 2, which consists of four modules: Input and output of vehicle signal; Vehicle model; Vehicle mass estimation based on EH∞KF; and Vehicle state estimation based on EH∞KF. The vehicle model receives the input signals including front wheel angle and lateral acceleration. Then, the sensors transmit the measurement signals with noise uncertainty and model parameter perturbation to the next estimators. The first EH∞KF estimator is used to identify the mass parameter of the vehicle. Meanwhile, the second EH∞KF estimator uses the result of the first estimator to predict the vehicle state.

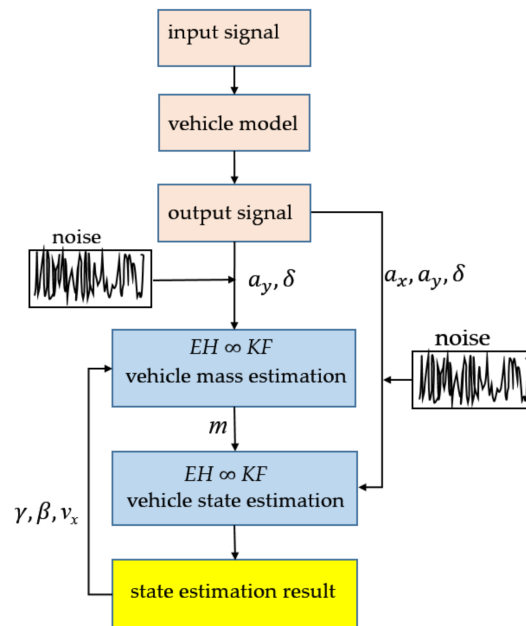


Figure 2. The framework of the proposed estimation algorithm.

3.1. EKF

The EKF algorithm is derived by firstly linearizing the nonlinear state and measurement equations, and then by using the standard Kalman filter [31]. The detailed process of the EKF is given as follows:

To linearize the nonlinear system state Equation (4), the results are as follows:

$$\begin{cases} x_{k+1} = Ax_k + u_k + w_k \\ y_k = Hx_k + v_k \end{cases} \tag{9}$$

where x_{k+1} is the system state variable; u_k is the input signal; y_{k+1} is the measured output; w_k and v_k separately is driving noise and measurement noise; both of which are uncorre-

lated white noises; Q and R are the noise covariance matrices; $\tilde{Z}_{m,k+1}$ is the vector of sensor measurement values; A and H separately are the Jacobian matrix where the nonlinear system state Equation (4) takes the partial derivatives to the state vector x_k :

$$\begin{aligned}
 A &= \frac{\partial f(x_k, u_k)}{\partial x_k} = \begin{bmatrix} \frac{\partial f_1}{\partial x_1} & \dots & \frac{\partial f_1}{\partial x_m} \\ \dots & \dots & \dots \\ \frac{\partial f_m}{\partial x_1} & \dots & \frac{\partial f_m}{\partial x_m} \\ \frac{\partial h_1}{\partial x_1} & \dots & \frac{\partial h_1}{\partial x_m} \\ \dots & \dots & \dots \\ \frac{\partial h_m}{\partial x_1} & \dots & \frac{\partial h_m}{\partial x_m} \end{bmatrix} \\
 H &= \frac{\partial h(x_k, u_k)}{\partial x_k} = \begin{bmatrix} \dots & \dots & \dots \\ \dots & \dots & \dots \end{bmatrix}
 \end{aligned}
 \tag{10}$$

Applying the basic equation of KF to the linearized model (9), the recursion algorithm of EKF is listed below.

The first step: prediction of the state variable at time k :

$$x_{k+1} = Ax_k + u_k \tag{11}$$

The second step: prediction of system state error matrix P :

$$P_{k+1} = AP_kA^T + Q \tag{12}$$

The third step: calculation of gain matrix K :

$$K_{k+1} = P_{k+1}H^T(HP_{k+1}H^T + R)^{-1} \tag{13}$$

The fourth step: update of system state variable \hat{X} at time is $k + 1$:

$$\hat{X}_{k+1} = X_{k+1} + K_{k+1}(\tilde{Z}_{m,k+1} - HX_{k+1}) \tag{14}$$

The fifth step: update of system state error covariance matrix \hat{P} :

$$\hat{P}_{k+1} = (I - K_{k+1}H^T)P_{k+1} \tag{15}$$

In Formulas (11) and (12), the initial value of state variable and system state error covariance matrix is separate $x_0 = E[x_0]$, $P_0 = \text{var}[x_0]$.

3.2. EH ∞ KF

The EH ∞ KF algorithm is a joint method that the nonlinear discrete-time systems are first linearized similar to the EKF and the linearization errors are treated as disturbances, and then the linear H ∞ filtering technique is directly applied to the linearized systems [32].

The discrete-time nonlinear dynamic model for the H ∞ filter is given as follows [33].

$$\begin{cases} x_{k+1} = f(x_k, u_k) + w_k \\ y_k = h(x_k, u_k) + v_k \end{cases} \tag{16}$$

where x_k is the state vector, u_k is the input signal, and y_k is the observation vector. w_k and v_k are respectively the process and measurement noise which are random and uncertain.

In the H ∞ filter approach, a linear combination of states is estimated instead of directly estimating the state.

$$z_k = L_k x_k \tag{17}$$

where z_k is the signal to be estimated and L_k is a known matrix that is assumed as $L_k = I$; I is an identity matrix.

The H ∞ filter defines a cost function as the performance measure [34].

$$J = \frac{\sum_{k=0}^{N-1} \|z_k - \hat{z}_k\|_{S_k}^2}{\|x_0 - \hat{x}_0\|_{P_0}^2 + \sum_{k=0}^{N-1} (\|w_k\|_{Q_k}^2 + \|v_k\|_{R_k}^2)} \tag{18}$$

where \hat{x}_0 is defined as the estimation of the initial state, $x_0 - \hat{x}_0$ is unknown initial estimation error. Herein, \hat{z}_k is defined as the estimation of z_k , $z_k - \hat{z}_k$ is defined as the estimation error, $\|z_k - \hat{z}_k\|_{S_k}^2$ denotes the weighted inner product, as well as the other analogous symbols. The symmetric positive definite matrices P_0, Q_k, R_k, S_k are unknown that should be chosen by designers based on the specific applications. Especially, S_k will affect the gain matrix in the H ∞ filter.

The objective of the H ∞ filter algorithm is to guarantee the finite upper bound on the estimation error and simultaneously minimize this upper bound [35].

$$\sup J < \frac{1}{\theta} \tag{19}$$

where ‘‘sup’’ is supremum, θ is a predefined scalar constant, and the error attenuation parameter. Neglecting the supremum and according to Equations (18) and (19), results in the following:

$$J = \sum_{k=0}^{N-1} \|z_k - \hat{z}_k\|_{S_k}^2 - \frac{1}{\theta} [\sum_{k=0}^{N-1} (\|w_k\|_{Q_k}^2 + \|v_k\|_{R_k}^2)] - \frac{1}{\theta} \|x_0 - \hat{x}_0\|_{P_0}^2 < 0 \tag{20}$$

Based on (17) and (19), the designer may select suitable estimation \hat{x}_k to minimize J , and then select suitable w_k, v_k, x_0 to maximize J , so the H ∞ filter can be interpreted as the following ‘‘mini-max’’ problem:

$$J^* = \min_{\hat{x}_k} \max_{w_k, v_k, x_0} J \tag{21}$$

In this paper, combining EKF with H ∞ filter, the recursion algorithm of EH ∞ KF can be expressed by the following steps:

$$x_{k|k-1} = A_k x_{k-1|k-1} + w_k \tag{22}$$

$$y_{k|k-1} = H_k x_{k|k-1} + v_k \tag{23}$$

$$P_{k|k-1} = A_k P_{k-1|k-1} A_k^T + Q_k \tag{24}$$

$$K_k = P_{k|k-1} [I - \theta S_k P_{k|k-1} + H_k^T R_k^{-1} H_k P_{k|k-1}]^{-1} H_k^T R_k^{-1} \tag{25}$$

$$\hat{x}_{k|k} = A_k x_{k|k-1} + A_k K_k (y_{k|k} - H_k x_{k|k-1}) \tag{26}$$

$$\hat{P}_{k|k} = A_k P_{k|k-1} [I - \theta S_k P_{k|k-1} + H_k^T R_k^{-1} H_k P_{k|k-1}]^{-1} A_k^T + Q_k \tag{27}$$

where A_k and H_k are respectively Jacobian matrix. Formulas (22)–(24) are a prediction of the state variable, measurement, and error covariance matrix at time $k - 1$. Formula (25) stands for the calculation of the gain matrix K , and Formulas (26) and (27) are respectively the update of system state and error covariance matrix at time k .

In Equation (27), the term $\theta S_k P_{k|k-1}$ tends to make $\hat{P}_{k|k}$ larger, as well as K_k , which increases the weight of measurement. Compared with the EKF, the EH ∞ KF adds the tolerance to the uncertain dynamics model and noise so that it has stronger robustness than the EKF. In addition, the following circumstance must be satisfied to make sure the EH ∞ KF algorithm can be realized successfully when θ is selected [25]:

$$P_{k|k-1}^{-1} - \theta S_k + H_k^T R_k^{-1} H_k > 0 \tag{28}$$

3.3. $EH^\infty KF$ Based Vehicle Mass and State Joint Estimation

Figure 3 is the flowchart of $EH^\infty KF$ based vehicle mass and state estimation. An $EH^\infty KF$ estimates the vehicle mass in real-time to cope with the uncertainty of the model parameters, and secondly, the output of this $EH^\infty KF$ is used as input to another $EH^\infty KF$ to estimate the vehicle state in real-time. The specific iterative process of $EH^\infty KF$ is as follows.

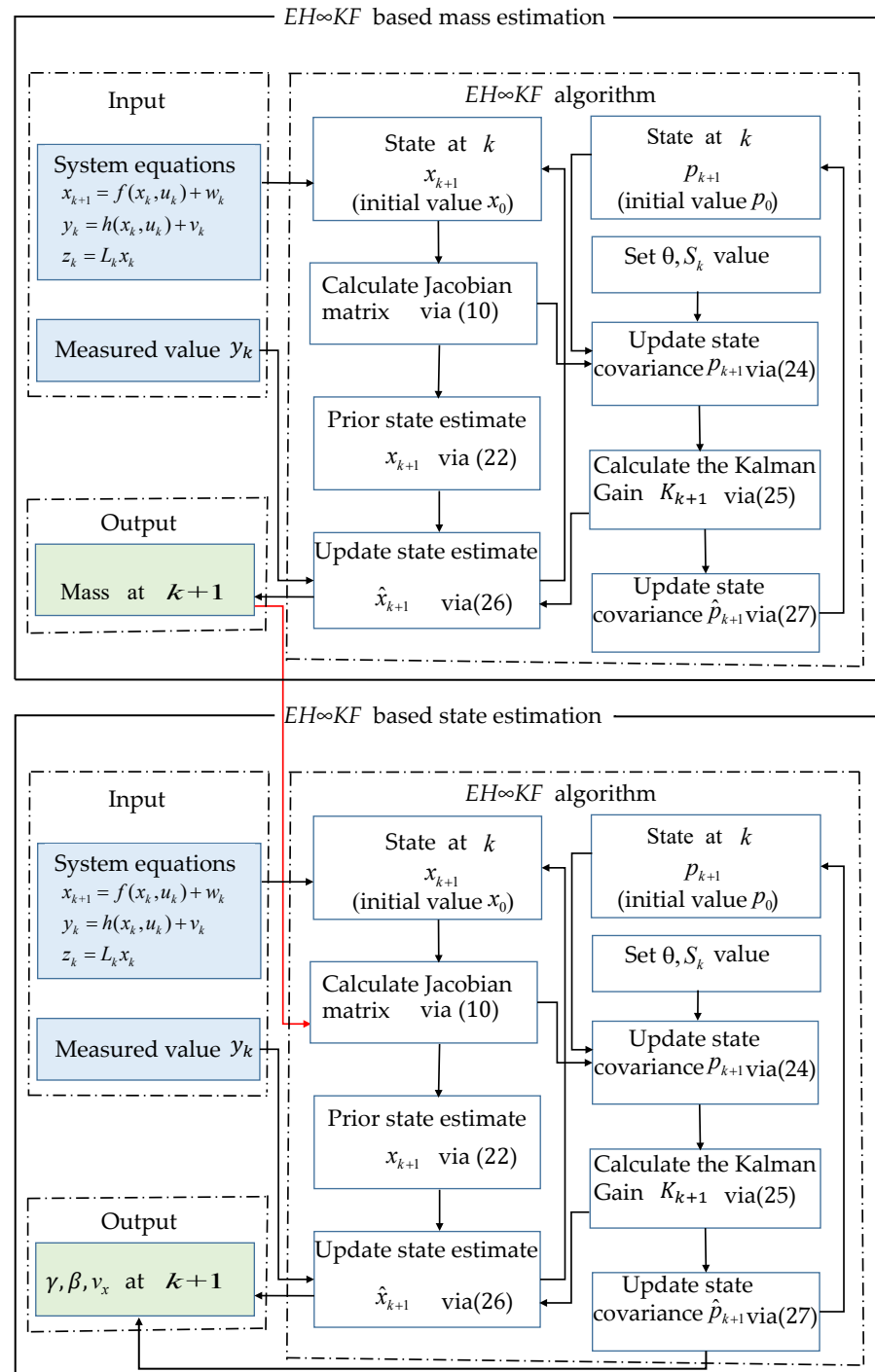


Figure 3. The joint estimation framework.

We first calculate the prior estimate and the estimation error covariance based on the known initial values. Then, the estimation error covariance of the prior state is used to update Kalman gain. Next, the posterior state is calculated using the Kalman gain and the prior state. Finally, the posterior state error covariance is dynamically updated using

Equation (27). The above iterative steps will continuously loop to obtain accurate vehicle state information.

4. Simulation Experiment Platform and Results

The proposed comprehensive estimation schemes implemented in MATLAB/Carsim co-simulation experiment platform are presented in this section. The MATLAB software is used to run the EH ∞ KF algorithm and the Carsim software is utilized to set up the test traffic scenario of the double lane change. Herein, this section provides two test examples to demonstrate the effectiveness of the proposed method. In addition, the traditional EKF and the proposed estimation method are compared respectively with the reference value.

4.1. The Simulation Experiment Platform

The simulative experimental platform is shown as Figure 4, which is composed of the following three subsystems:

1. The Vehicle Simulation System: It contains two parts: the Driver Model and the Carsim Model. The Driver Model can regulate the steering angle, driving, and braking pedals to follow the target trajectory and target speed. Afterward, the signals of the Steering-wheel Angle Sensor, Accelerator Position Sensor, and Brake Position Sensor are transferred to the Carsim model. Meanwhile, the Carsim model feedbacks the vehicle state x_k to the driver model;
2. The Data Acquisition System: It simulates the vehicle measurement system. Firstly, the observation variables (a_x, a_y, δ) from the vehicle model are collected by the virtual sensors. Simultaneously, the Non-Gaussian measurement noise v_k that simulates the real sensors is added to the actual output observation vectors. Finally, the virtual sensors will pass the measurements to the State Estimation System;
3. The State Estimation System is the focus of the simulative experimental platform. It can use the EH ∞ KF estimator to estimate the vehicle mass, and then take the vehicle mass as the input variable of the next EH ∞ KF estimator. The last estimation results (m, γ, β, v_x) will compare respectively to the reference vehicle mass and state vectors given by the Carsim Model system.

4.2. Simulation Results

Two different test scenarios were set up to verify the effectiveness of the proposed algorithm: they are the double lane change test on high and low adhesion surfaces, respectively. The vehicle state output values from the software Carsim are used as reference values to compare with the proposed algorithm. The vehicle model parameters from the Carsim software are shown in Table 1

Table 1. The parameters of vehicle model.

Symbol	Name	Numbers and Units
m	mass	1420 kg
a	distance from the center of gravity to the front axle	1.015 m
b	distance from the center of gravity to the rear axle	1.895 m
I_z	vehicle moment of inertia about z axis	1536.7 kg·m ²
k_1	cornering stiffness of the front axle	−102,540 N/rad
k_2	cornering stiffness of the rear axle	−98,500 N/rad

4.2.1. Double Lane Change Test on High Friction Coefficient Road

Figure 5 demonstrates a typical curve of the steering wheel angle on the dry asphalt road in which the tire-road friction coefficient is 0.85 and the initial vehicle speed is 40 km/h. Since the Carsim software provides a manual input interface, we can directly simulate the scenario by giving the specific parameters for the above conditions. It is taken as the input to the vehicle mass estimation. To verify the effectiveness of the vehicle mass

estimation algorithm, we set up the initial vehicle mass to be 1000 kg, while the real vehicle mass is 1420 kg. The simulation time is set to 20 s. The estimation results of vehicle mass are demonstrated in Figure 6. In Figure 6, the vehicle mass estimation curve of the EKF algorithm rises rapidly after 5.5 s. After about 12.5 s, the vehicle mass estimation converges to 1250 kg. It is obvious that there is a difference of 170 kg from the reference value. For the $EH\infty KF$ algorithm, the vehicle mass estimation curve rises rapidly after 6 s. The vehicle mass estimation converges quickly to 1400 kg after a small fluctuation about 7.7 s. The $EH\infty KF$ method is closer to the reference value than the EKF method under the above conditions.

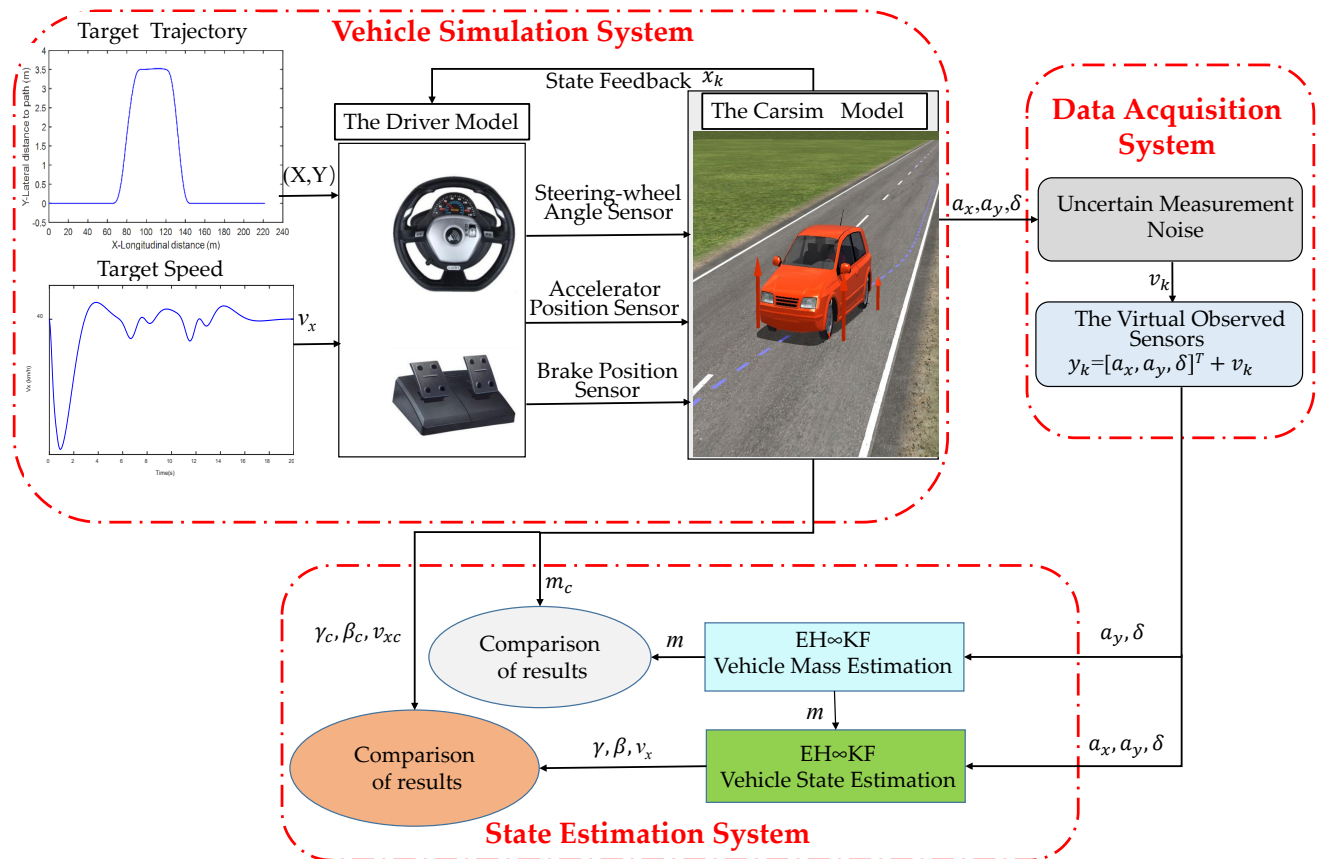


Figure 4. The co-simulation environment is used for validation of the proposed algorithm.

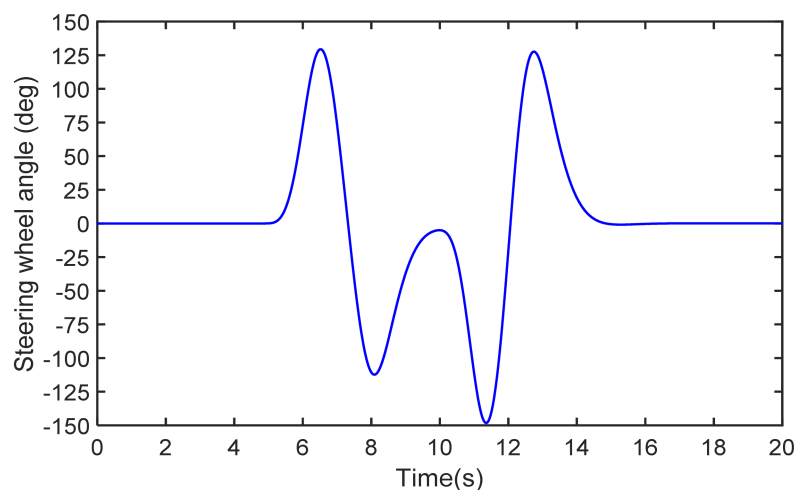


Figure 5. The steering-wheel angle on high friction coefficient road.

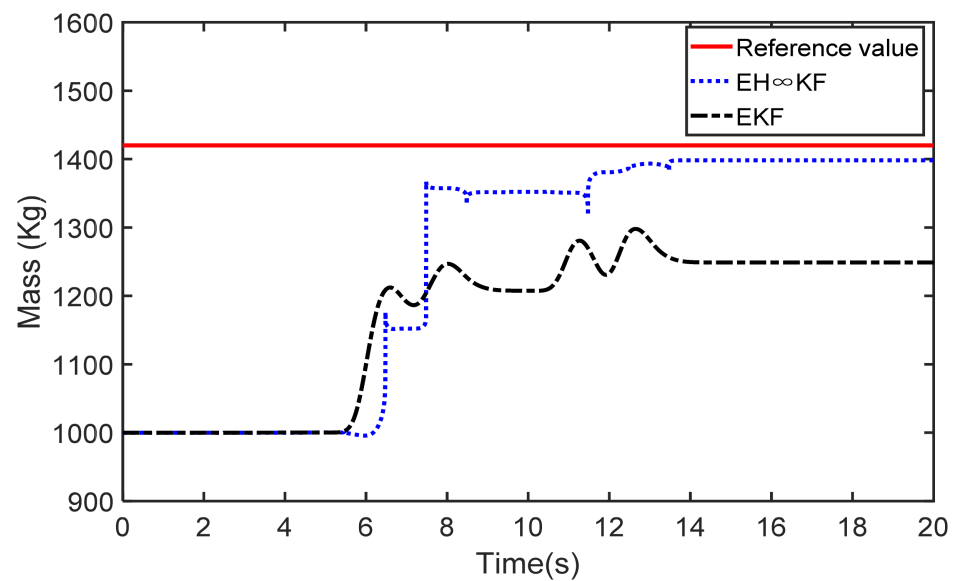


Figure 6. Vehicle mass estimation on high friction coefficient road.

Figures 7–9 show the estimation results of yaw rate, sideslip angle, and vehicle speed using the EKF and the $\text{EH}\infty\text{KF}$ on high friction coefficient road. According to the figures, it can be noticed that the yaw rate, sideslip angle, and vehicle speed estimation curves of the $\text{EH}\infty\text{KF}$ follow reference values better during the simulation process. Nevertheless, the estimation curves of the EKF are far from the reference value. From the locally enlarged view in Figures 7 and 8, it can be seen that the effect of $\text{EH}\infty\text{KF}$ is better than EKF. In Figure 9, the vehicle speed estimation using the EKF has a large fluctuation at the moment of the 6 s, and a huge estimation deviation with a reference value from the 6 s to the 20 s. From Figures 10–12, we can see that the mean absolute error of vehicle state estimation using the $\text{EH}\infty\text{KF}$ is lower than the EKF. The RMSE index of the vehicle state is shown in Table 2. The $\text{EH}\infty\text{KF}$ consistently outperforms the EKF. In summary, the estimation performance of the $\text{EH}\infty\text{KF}$ is better than standard EKF under the above conditions.

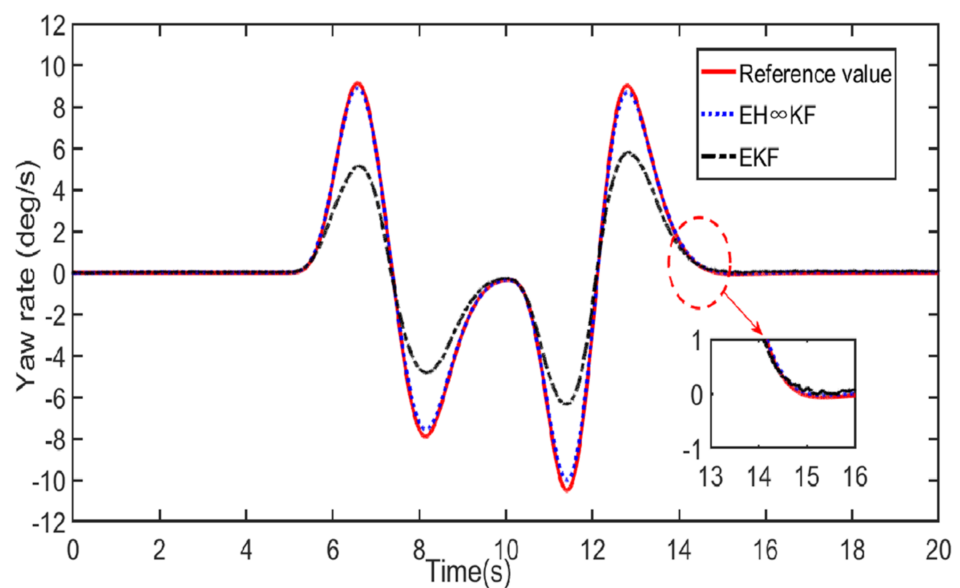


Figure 7. Yaw rate estimation on high friction coefficient road.

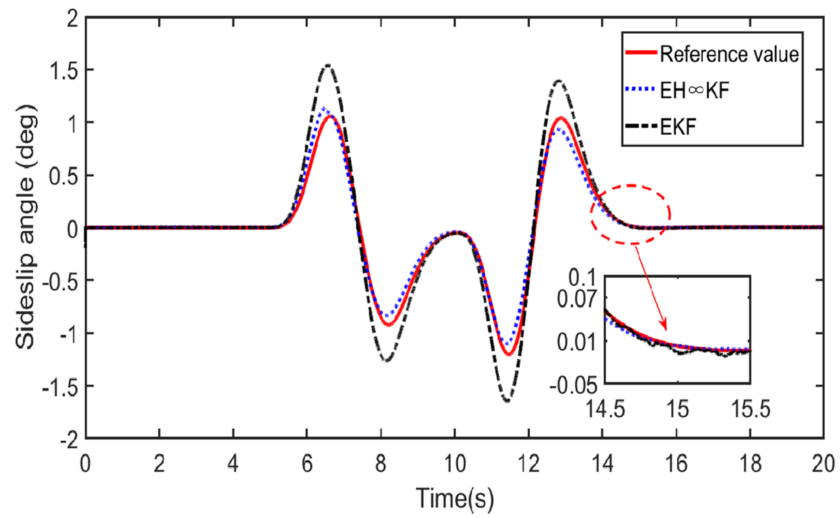


Figure 8. Sideslip angle estimation on high friction coefficient road.

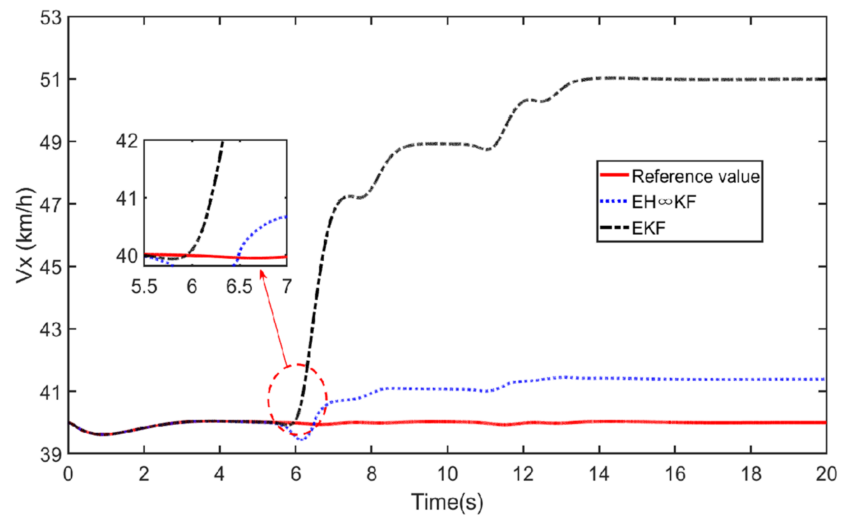


Figure 9. Vehicle speed estimation on high friction coefficient road.

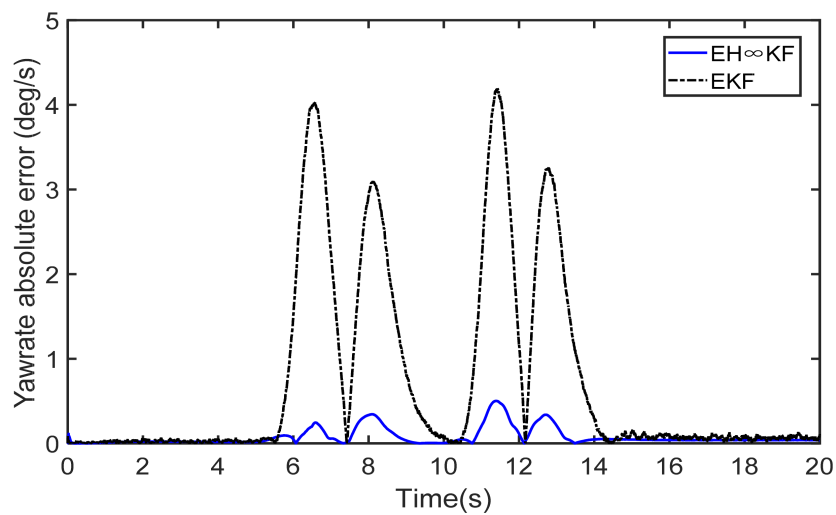


Figure 10. Yaw rate absolute error on high friction coefficient road.

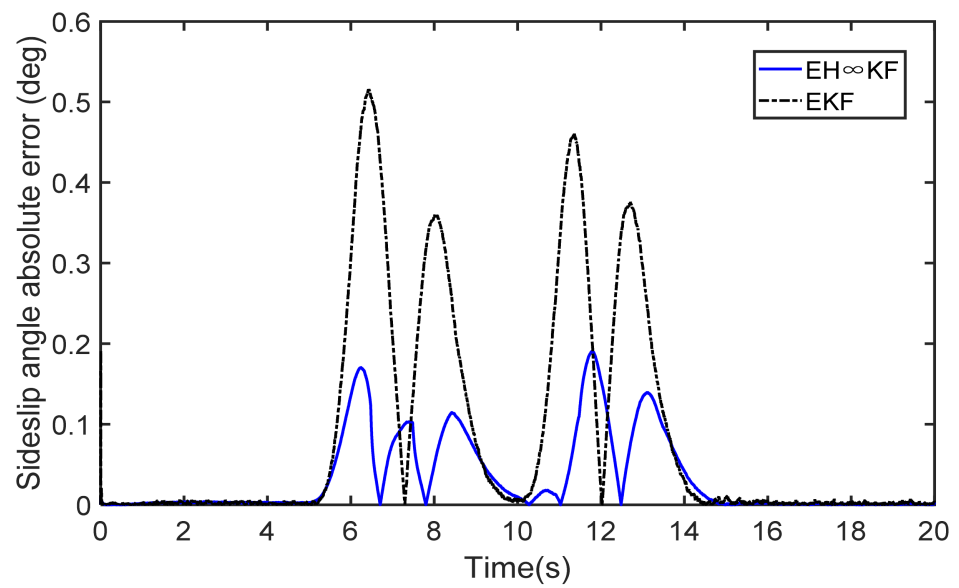


Figure 11. Sideslip angle absolute error on high friction coefficient.

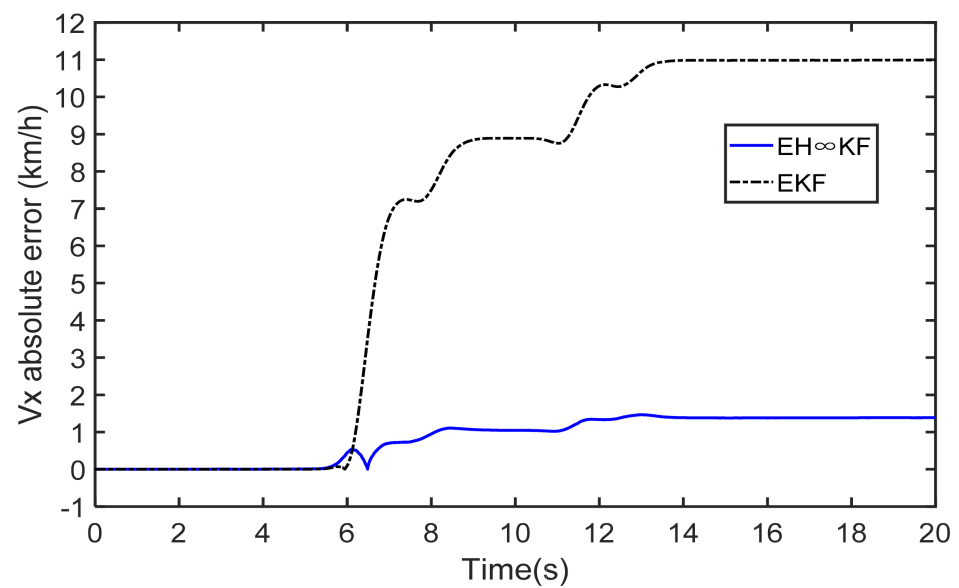


Figure 12. Vehicle speed absolute error on high friction coefficient road.

Table 2. RMSE of estimation results on high friction coefficient road.

RMSE	Yaw Rate	Sideslip Angle	Vehicle Speed
EKF	1.3775	0.1658	8.1780
$E_{H\infty}KF$	0.1267	0.0583	1.0275

4.2.2. Double Lane Change Test on Low Friction Coefficient Road

Figure 13 shows a typical curve of the steering wheel angle on the ice-snow road that is taken similarly as the input signal to the vehicle mass estimator. The tire–road friction coefficient is 0.2 and the initial vehicle speed is 20 km/h. Herein, the initial vehicle mass is identified as 1000 kg, while the real vehicle mass is 1420 kg. The simulation time is set to 20 s.

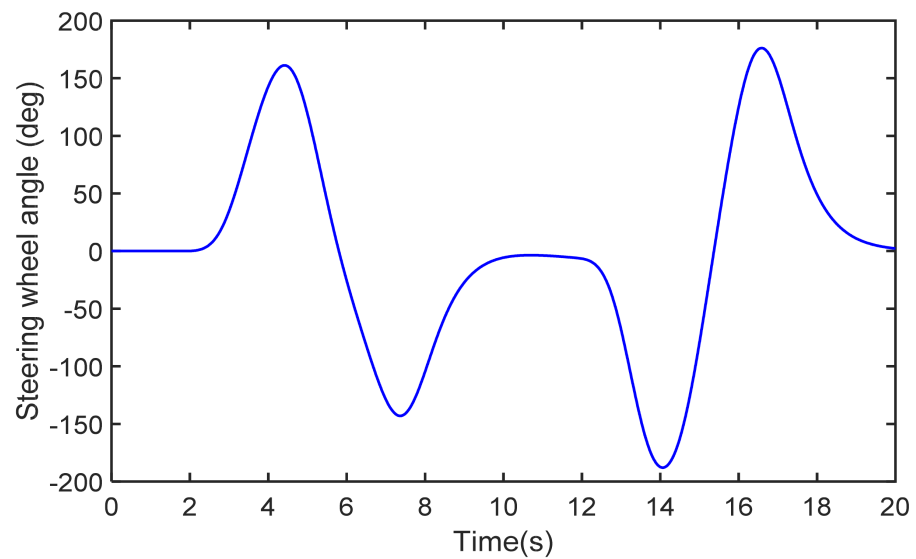


Figure 13. The steering-wheel angle on low friction coefficient road.

Figure 14 demonstrates the estimation results of vehicle mass based separately on EKF and $EH\infty KF$ methods. As described in Figure 14, the vehicle mass estimation curve of the EKF algorithm rises rapidly after 2 s. After about 18 s, the vehicle mass estimation based on the EKF algorithm converges to 1350 kg. It is obvious that there is a difference of 70 kg from the reference value. For the $EH\infty KF$ algorithm, the vehicle mass estimation curve rises rapidly after 3.5 s. The vehicle mass estimation converges quickly to 1380 kg after 6 s. At the moment of 14 s, the vehicle mass estimation curve of the $EH\infty KF$ fluctuates again. The vehicle mass estimation converges quickly to 1422 kg at the moment of 16 s. The $EH\infty KF$ method is closer to the reference value than the EKF method under the above conditions.

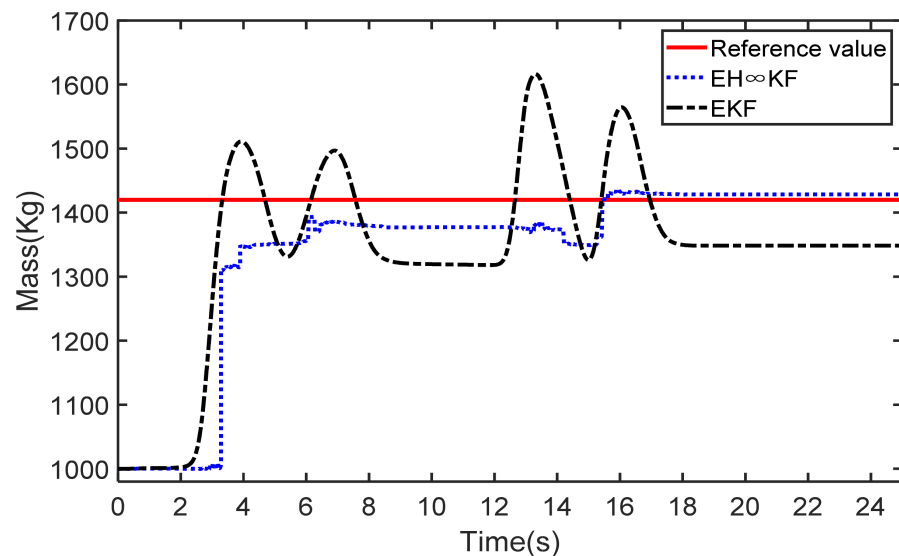


Figure 14. Vehicle mass estimation on low friction coefficient road.

The estimation results of yaw rate, sideslip angle, and vehicle speed using the EKF and the $EH\infty KF$ on low friction coefficient road are shown in Figures 15–17. As these figures show, during the simulation process, the yaw rate and sideslip angle estimation curves of the $EH\infty KF$ are closer to the reference value comparing with the EKF. Especially in Figure 17, the vehicle speed estimation curve of the EKF cannot follow the reference value better, the vehicle speed estimation using the EKF has a large fluctuation at the moment of the 1.5 s, and a huge estimation deviation with reference value after about 3.5 s. On the

other hand, from the locally enlarged view in Figures 15 and 16, it can be seen that the effect of EH ∞ KF is better than EKF. From Figures 18–20, we can see that the mean absolute error of vehicle state estimation using the EH ∞ KF is lower than the EKF. The RMSE index of the vehicle state is shown in Table 3. The EH ∞ KF consistently outperforms the EKF. Based on the simulation results above, we can see that the proposed method demonstrates higher precision than the traditional EKF method when system noise and model parameters are uncertain at the same time.

Table 3. RMSE of estimation results on low friction coefficient road.

RMSE	Yaw Rate	Sideslip Angle	Vehicle Speed
EKF	0.2797	0.0619	1.4126
EH ∞ KF	0.0336	0.0190	0.1943

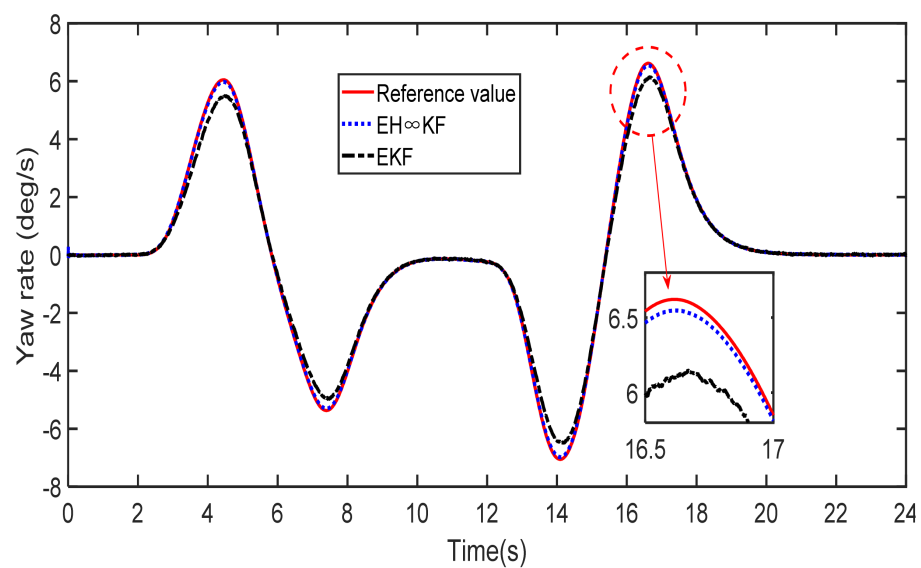


Figure 15. Yaw rate estimation on low friction coefficient road.

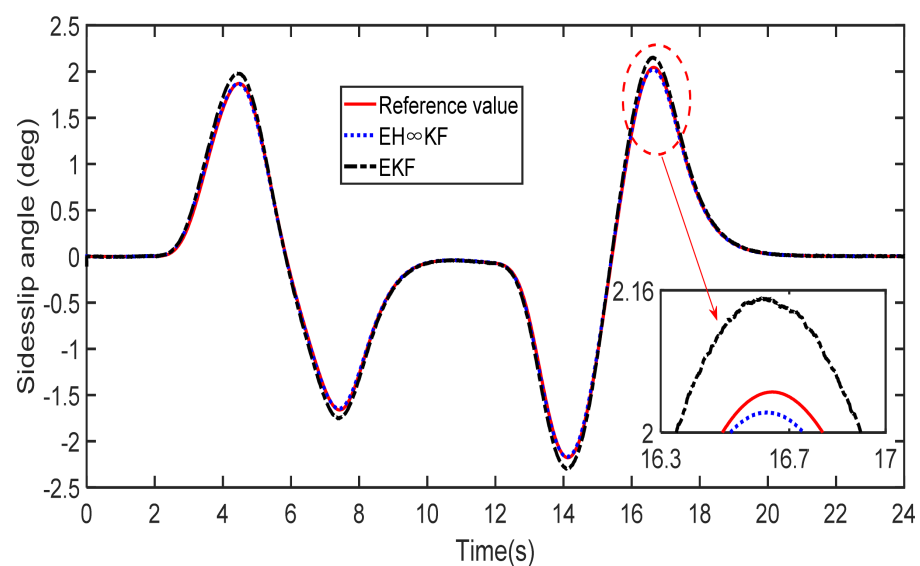


Figure 16. Sideslip angle estimation on low friction coefficient road.

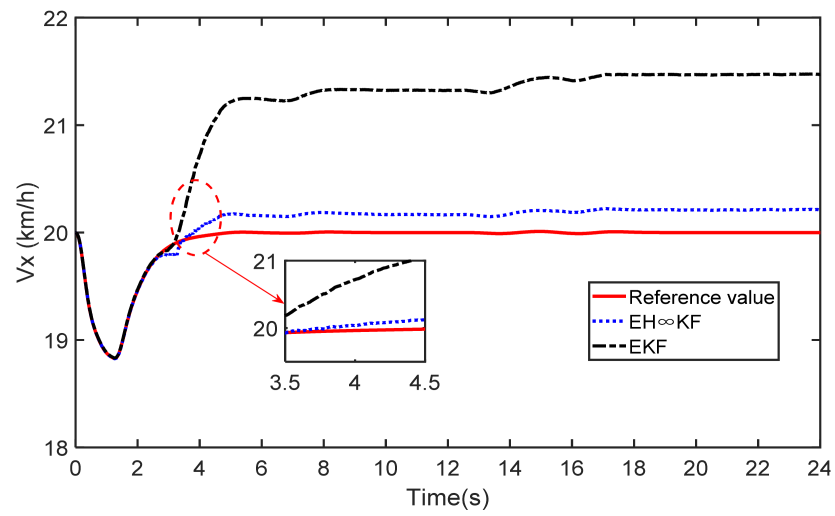


Figure 17. Vehicle speed absolute error on low friction coefficient road.

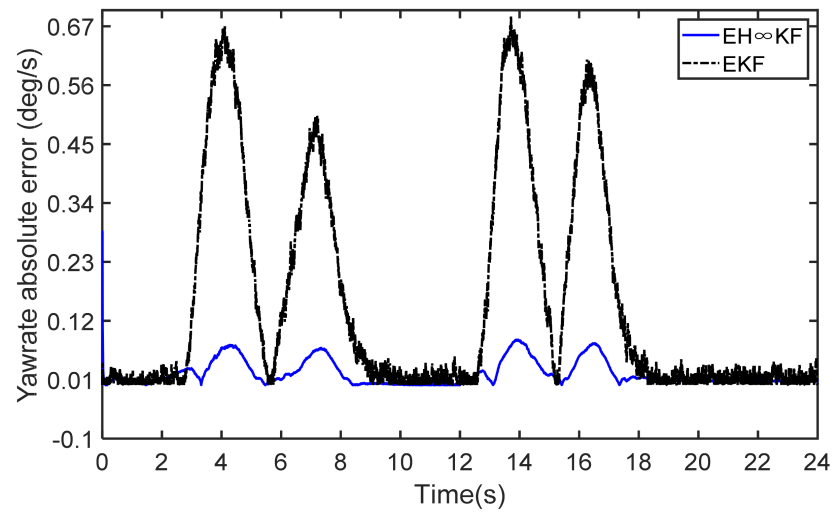


Figure 18. Yaw rate absolute error on low friction coefficient road.

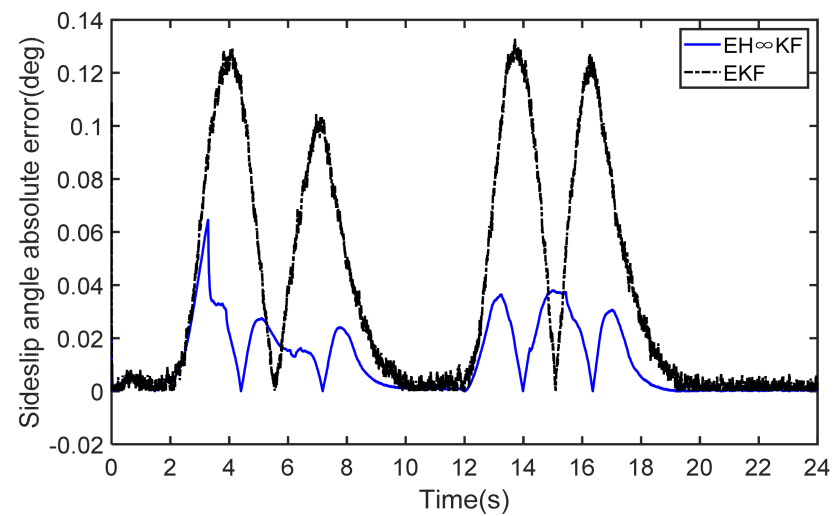


Figure 19. Sideslip angle absolute error on low friction coefficient road.

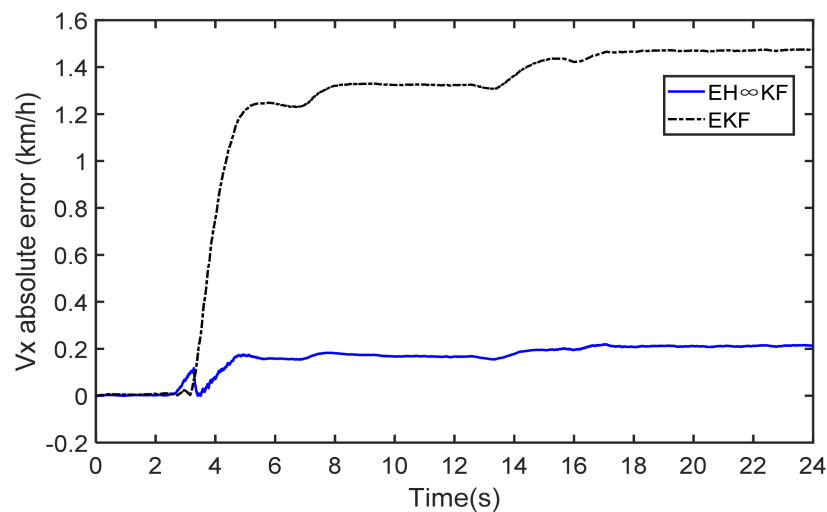


Figure 20. Vehicle speed absolute error on low friction coefficient road.

5. Conclusions

In this paper, a comprehensive estimation scheme is proposed to estimate vehicle state when the noise statistics are unknown and model parameters are inaccurate. The test results indicate that the proposed method has higher estimation accuracy than the existing EKF method. Nevertheless, there are some limitations to this study. We neglect the effect of the road-bank angle in this study. In addition, verification of the algorithm in more complex driving scenarios will also further highlight the superiority of our approach. We will consider the above issues and further optimize our algorithm to improve the estimation accuracy in our future work.

Author Contributions: Conceptualization, F.Z. and G.Y.; model, F.Z. and Y.W.; methodology, F.Z., Y.W. and J.H.; experiment platform, F.Z., G.Y., and H.Z.; formal analysis, F.Z. and S.C.; resources, G.Y. and Y.W.; writing—original draft preparation, F.Z.; writing—review and editing, F.Z., J.H., and D.Z.; supervision, G.Y.; project administration, F.Z., G.Y., and S.C.; funding acquisition, F.Z. and G.Y. All authors have read and agreed to the published version of the manuscript.

Funding: This research was supported in part by National Natural Science Funds for Distinguished Young Scholar under Grant 52025121; in part by the National Natural Science Foundation of China under Grant 51975118; in part by Basic Research Project of Changzhou Science and Technology Plan under Grant CJ20190009; in part by the Higher Vocational College Teacher Professional Leader High-end Training Project in Jiangsu Province under Grant 2019GRFX014; and in part by Qing Lan Project in Jiangsu Province under Grant 202010.

Conflicts of Interest: The authors declare no conflict of interest.

References

- Xu, Q.; Zhou, C.; Huang, H.; Zhang, X. Research on the Coordinated Control of Regenerative Braking System and ABS in Hybrid Electric Vehicle Based on Composite Structure Motor. *Electronics* **2021**, *10*, 223. [[CrossRef](#)]
- Ahangarnejad, A.H.; Radmehr, A.; Ahmadian, M. A review of vehicle active safety control methods: From antilock brakes to semiautonomy. *J. Vib. Control* **2020**, 1–30. [[CrossRef](#)]
- Wang, Y.; Yin, G.; Li, Y.; Ullah, S.; Zhuang, W.; Wang, J.; Zhang, N.; Geng, K. Self-learning control for coordinated collision avoidance of automated vehicles. *Proc. Inst. Mech. Eng. Part D J. Automob. Eng.* **2021**, *235*, 1149–1163. [[CrossRef](#)]
- Wang, Y.; Geng, K.; Xu, L.; Ren, Y.; Dong, H.; Yin, G. Estimation of Sideslip Angle and Tire Cornering Stiffness Using Fuzzy Adaptive Robust Cubature Kalman Filter. *IEEE Trans. Syst. Man Cybern. Syst.* **2020**, 1–12. [[CrossRef](#)]
- Tin Leung, K.; Whidborne, J.F.; Purdy, D.; Dunoyer, A. A review of ground vehicle dynamic state estimations utilizing GPS/INS. *Veh. Syst. Dyn.* **2011**, *49*, 29–58. [[CrossRef](#)]
- Baffet, G.; Charara, A.; Lechner, D. Estimation of vehicle sideslip, tire force, and wheel cornering stiffness. *Control Eng. Pract.* **2009**, *17*, 1255–1264. [[CrossRef](#)]

7. Chen, T.; Xu, X.; Chen, L.; Jiang, H.; Cai, Y.; Li, Y. Estimation of longitudinal force, lateral vehicle speed, and yaw rate for four-wheel independent driven electric vehicles. *Mech. Syst. Signal Process.* **2018**, *101*, 377–388. [[CrossRef](#)]
8. Zhu, H.; Li, L.; Jin, M.; Li, H.; Song, J. Real-time yaw rate prediction based on a non-linear model and feedback compensation for vehicle dynamics control. *Proc. Inst. Mech. Eng. D J. Automob. Eng.* **2013**, *227*, 1431–1445. [[CrossRef](#)]
9. Ma, H.; Yan, L.; Xia, Y.; Fu, M. *Kalman Filtering and Information Fusion*, 1st ed.; Springer: Singapore, 2020; pp. 1–8.
10. Chui, C.K.; Chen, G. *Kalman Filtering*, 5th ed.; Springer International Publishing: Berlin, Germany, 2017; pp. 19–26.
11. Li, Q.; Li, R.; Ji, K.; Dai, W. Kalman filter and its application. In Proceedings of the 2015 8th International Conference on Intelligent Networks and Intelligent Systems (ICINIS), Tianjin, China, 1–3 November 2015; pp. 74–77.
12. Li, X.L.; Zhu, Y.M.; Wang, J.; Han, C.Z. Optimal linear estimation fusion-PartI: Unified fusion rules. *IEEE Trans. Inf. Theory* **2003**, *49*, 2192–2208. [[CrossRef](#)]
13. Liu, W.Q.; Wang, X.M.; Deng, Z.L. Robust centralized and weighted measurement fusion Kalman estimators for uncertain multisensor systems with linearly correlated white noises. *Inf. Fusion* **2017**, *35*, 11–25. [[CrossRef](#)]
14. Zhu, J.; Park, J.H.; Lee, K.S.; Spiriyagin, M. Robust extended Kalman filter of discrete-time Markovian jump nonlinear system under uncertain noise. *J. Mech. Sci. Technol.* **2008**, *22*, 1132–1139. [[CrossRef](#)]
15. Nardone, S.C.; Lindgren, A.G.; Gong, K.F. Sept. Fundamental properties and performance of conventional bearings-only target motion analysis. *IEEE Trans. Autom. Control* **1984**, *29*, 775–787. [[CrossRef](#)]
16. Toloei, A.; Niazi, S. State estimation for target tracking problems with nonlinear Kalman filter algorithms. *Int. J. Comput. Appl.* **2014**, *98*, 30–36. [[CrossRef](#)]
17. Wang, Y.; Xu, L.; Zhang, J.; Dong, H.; Liu, Y.; Yin, G. An Adaptive Fault-Tolerant EKF for Vehicle States Estimation with Multiple Partial Missing Measurements. *IEEE/ASME Trans. Mechatron.* **2021**, 1–10. [[CrossRef](#)]
18. Hrgetic, M.; Deur, J.; Ivanovic, V.; Tseng, E. Vehicle sideslip angle estimator based on nonlinear vehicle dynamics model and stochastic tire forces modeling. *SAE Int. J. Passeng. Cars-Mech. Syst.* **2014**, *7*, 86–95. [[CrossRef](#)]
19. Doumiati, M.; Victorino, A.C.; Charara, A.; Lechner, D. Onboard real-time estimation of vehicle lateral tire-road forces and sideslip angle. *IEEE/ASME Trans. Mechatron.* **2011**, *16*, 601–614. [[CrossRef](#)]
20. Wenzel, T.A.; Burnham, K.J.; Blundell, M.V.; Williams, R.A.; Fairgrieve, A. Simplified extended Kalman filter for automotive state estimation. *Int. J. Model. Identif. Control* **2008**, *3*, 201–211. [[CrossRef](#)]
21. Wada, M.; Yoon, K.S.; Hashimoto, H. High accuracy road vehicle state estimation using extended Kalman filter. In Proceedings of the 2000 IEEE Intelligent Transportation Systems Conference (ITSC), Dearborn, MI, USA, 1–3 October 2000; pp. 282–287.
22. Baek, S.; Liu, C.; Watta, P.; Murphey, Y.L. Accurate vehicle position estimation using a Kalman filter and neural network-based approach. In Proceedings of the 2017 IEEE Symposium Series on Computational Intelligence, Honolulu, HI, USA, 27 November–1 December 2017; pp. 1–8.
23. Patra, N.; Sadhu, S. Adaptive Extended Kalman filter for the state estimation of Anti-lock Braking system. In Proceedings of the 2015 Annual IEEE India Conference (INDICON), New Delhi, India, 17–20 December 2015; pp. 1–6.
24. Hashlamon, I. A new adaptive extended Kalman filter for a class of nonlinear systems. *J. Appl. Comput. Mech.* **2020**, *6*, 1–12.
25. Lin, C.; Gong, X.; Xiong, R.; Cheng, X. A novel H_∞ and EKF joint estimation method for determining the center of gravity position of electric vehicles. *Appl. Energy* **2017**, *194*, 609–616. [[CrossRef](#)]
26. Montonen, J.; Nevaranta, N.; Lindh, T.; Alho, J.; Immonen, P.; Pyrhönen, O. Experimental Identification and Parameter Estimation of the Mechanical Driveline of a Hybrid Bus. *IEEE Trans. Ind. Electron.* **2017**, *65*, 5921–5930. [[CrossRef](#)]
27. Nevaranta, N.; Montonen, J.H.; Lindh, T. Online Estimation of a Mechanical Driveline Parameters of a Hybrid Bus. In Proceedings of the 2018 20th European Conference on Power Electronics and Applications (EPE'18 ECCE Europe), Riga, Latvia, 17–21 September 2018; pp. P.1–P.7.
28. Wenzel, T.A.; Burnham, K.J.; Blundell, M.V.; Williams, R.A. Dual extended Kalman filter for vehicle state and parameter estimation. *Veh. Syst. Dyn.* **2007**, *44*, 153–171. [[CrossRef](#)]
29. Chen, B.-C.; Hsieh, F.-C. Sideslip angle estimation using extended Kalman filter. *Veh. Syst. Dyn.* **2009**, *46*, 353–364. [[CrossRef](#)]
30. Wang, Y.; Zhang, F.; Geng, K.; Zhuang, W.; Dong, H.; Yin, G. Estimation of Vehicle State Using Robust Cubature Kalman Filter. In Proceedings of the 2020 IEEE/ASME International Conference on Advanced Intelligent Mechatronics (AIM), Boston, MA, USA, 6–9 July 2020; pp. 1024–1029.
31. Wang, X.; Zhang, H.; Jiang, X.; Yang, Y. Target tracking based on the extended H-infinity filter in wireless sensor networks. *J. Control. Theory Appl.* **2011**, *9*, 479–486. [[CrossRef](#)]
32. Einicke, G.A.; White, L.B. The extended H_∞ filter—A robust EKF. In Proceedings of the 1994 IEEE International Conference on Acoustics, Speech, and Signal Processing, Adelaide, SA, Australia, 19–22 April 1994; pp. 2595–2599.
33. Chandra, K.P.B.; Gu, D.-W.; Postlethwaite, I. Fusion of an extended h_∞ filter and cubature Kalman filter. *IFAC Proc. Vol.* **2011**, *44*, 9091–9096. [[CrossRef](#)]
34. Simon, D. *Optimal State Estimation: Kalman, H Infinity, and Nonlinear Approaches*, 1st ed.; John Wiley & Sons, Inc.: Hoboken, NJ, USA, 2006; pp. 343–347.
35. Zhao, J. Dynamic State Estimation With Model Uncertainties Using H_∞ Extended Kalman Filter. *IEEE Trans. Power Syst.* **2017**, *33*, 1099–1100. [[CrossRef](#)]